Dual-Band Leaky-Wave Antenna Based on Dual-Mode Composite Microstrip Line for Microwave and Millimeter-Wave Applications

Yujian Li, *Member, IEEE*, and Junhong Wang, *Senior Member, IEEE*

***Abstract*— A dual-mode composite microstrip line (DMC-MSL) is reported in this paper for the purpose of designing dual-band antennas and devices with a large frequency ratio. The metallic strip of the conventional MSL is replaced with a substrate integrated waveguide (SIW) arranged into a thin dielectric laminate, which leads to that two modes operating in different frequency bands, i.e., the quasi-TEM mode and the TE_{10}-like mode, can propagate along the transmission line structure simultaneously. The DMC-MSL with a dual-layered planar configuration combines the merits of the MSL and the SIW. In addition, by adjusting the permittivity of the dielectric laminate used for realizing the thin SIW, the frequency ratio of the two operating modes can be varied flexibly. Based on the DMC-MSL structure, a novel dual-band leaky-wave antenna is presented. Periodic parasitic microstrip patches and the transverse slot array etched on the SIW are introduced in order to generate the required spatial harmonics. A feed structure that can excite the two operating modes of the DMC-MSL separately is designed as well. The fabricated prototype verifies that backward and forward frequency-scanning radiation beams are achieved within the low-frequency band from 5.75 to 8.5 GHz and the high-frequency band from 35 to 41.5 GHz, respectively. The proposed DMS-MSL structure and the leaky-wave antenna offer a new mean to implement antennas and devices for microwave and millimeter-wave dual-band applications.**

***Index Terms*— Dual-band, dual-mode composite microstrip line (DMC-MSL), frequency-scanning, leaky wave antenna, millimeter-wave.**

I. Introduction

DUAL-BAND and multi-band antennas are of great importance to modern wireless communication systems that operate in more than one frequency band, since they can save the volume occupied by the antennas, thus reducing the size of the entire system [1]–[4]. Nowadays, the operating bands of most wireless applications are assigned at low microwave frequencies. However, with the rapid development of the millimeter-wave technologies in recent years, microwave and millimeter-wave spectrums would be used together for the wireless communications with further improved performance in future. Therefore, the radiating elements that can work in microwave and millimeter-wave bands simultaneously would be a desirable candidate for these applications. Up to now, by integrating two or three types of radiating elements together, a few dual-band or triband antenna designs with a large frequency ratio have been investigated in the literature [5]–[10].

Due to the unique feature of beam scanning with the operating frequency and the simple feeding configuration, the leaky-wave antenna has been persistently studied, since it was invented. Its radiating mechanism has been explored systematically by many researchers [11]–[13]. Both the fundamental and higher order modes of a uniform transmission line with a longitudinal propagation constant of less than the wave number in free space or the spatial harmonics located in the fast-wave region that are excited by a periodic structure loading to a transmission line can be employed to implement the leaky-wave antenna. In recent years, by adopting the planar transmission lines, including the microstrip line (MSL) [14], [15] and the substrate integrated waveguide (SIW) [16]–[18], various leaky-wave antennas with low profile, ease of integration, and low fabrication costs have been reported for different wireless applications, such as radars [19], surveillance [20], real-time spectrum analyzers [21], and multipoint communications [22]. More recently, the leaky-wave antennas used for the fifth generation mobile communications [23] and the V-band millimeter-wave wireless applications [24] have also been studied.

In terms of the dual-band leaky wave antenna, several designs have also been investigated based on the composite right-/left-hand (CRLH) transmission line [25], [26], the mu-negative (MNG) transmission line [27], and the U-slot-loaded half-width MSL [28]. Unfortunately, the frequency ratio of the two bands is usually around or less than 2 in most reported dual-band leaky-wave antennas. It would be a constraint when the two operating bands with a large frequency ratio are demanded by the wireless applications.

Actually, all transmission line structures have their specific frequency bandwidth characterized by the required transmission quality throughout the band. The transmission lines supporting the TEM or quasi-TEM mode as the fundamental mode, including the coaxial cable, the MSL, and the coplanar waveguide (CPW), have cutoff frequency approaching zero,

Manuscript received July 12, 2017; revised December 14, 2017; accepted December 24, 2017. Date of publication February 1, 2018; date of current version April 5, 2018. This work was supported in part by the National Natural Science Foundation of China under Grant 61671052 and in part by the National Natural Science Foundation of China under Grant 61331002. *(Corresponding author: Yujian Li.)*

The authors are with the Institute of Lightwave Technology, Beijing Jiaotong University, Beijing 100044, China (e-mail: liyujian@bjtu.edu.cn).

Color versions of one or more of the figures in this paper are available online at http://ieeexplore.ieee.org.

Digital Object Identifier 10.1109/TAP.2018.2800705

so they are widely utilized for low-frequency applications. However, the undesired higher order mode would be excited along the transmission line with the increase of frequencies. Hence, these transmission lines have limitation on the highest operating frequency for fixed structure dimensions. On the other hand, nonzero cutoff frequencies can be found for transmission lines supporting the TE or TM mode as the operating mode, e.g., the air-filled waveguide and the SIW. In addition, due to possible existence of the higher order modes, the highest frequency limitation is also presented. In order to widen the limited frequency bandwidth, novel structures designated as the mode-selective and the mode-composite transmission lines have been reported very recently [29], [30]. Both the TEM mode and the TE_{10} mode can be excited separately in different frequency ranges, which results in that a much wider operating band or two bands can be realized by a transmission line structure.

In this paper, a new kind of the mode-composite transmission line is proposed. By replacing the metallic strip of the traditional MSL with a thin SIW, two operating modes can propagate along the structure simultaneously. Since the entire geometry of the proposed transmission line is still similar to the traditional MSL, it is named as the dual-mode composite MSL (DMC-MSL). The proposed DMC-MSL with a dual-layered configuration keeps the geometry advantages of the MSL, including ease of integration and a low profile. Furthermore, the frequency ratio of the two modes can be tuned flexibly in a large range by adjusting the relative dielectric constant of the substrate integrating the SIW. By employing the DMC-MSL, a novel dual-band leaky-wave antenna with a large frequency ratio of approximately 7 is then designed, fabricated, and tested to verify the proposed design. Frequency-scanning beams in backward and forward directions are realized, respectively, in the two bands. The proposed leaky-wave antenna would be an attractive candidate for future dual-band wireless applications at microwave and millimeter-wave frequencies.

This paper is organized as follows. The DMC-MSL is first presented in Section II. The design of the dual-band leaky-wave antenna and the feeding structure is depicted in Sections III and IV, respectively. Section V provides the measured results and discussions and a brief conclusion is finally given in Section VI.

II. Dual-Mode Composite Microstrip Line

A. Geometry

Geometry of the proposed DMC-MSL is illustrated in Fig. 1, where two substrates are stacked to construct the transmission line. The thickness of the Substrate 1 is much thinner than the counterpart of the Substrate 2. The SIW composed of the metallic strips and vias is integrated in Substrate 1 to operate as the metallic strip of the conventional MSL. Since there is no need of the interconnection between the two substrates, the DMC-MSL can be fabricated easily by applying glue or a dielectric bonding film to bond the two substrates together. Furthermore, the detailed dimensions of the DMC-MSL are presented in Fig. 1(b). In this paper, the

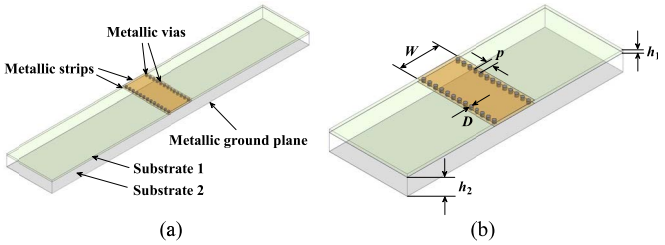

Fig. 1. Geometry of the proposed DMC-MSL. (a) Perspective view. (b) Geometry with dimensions.

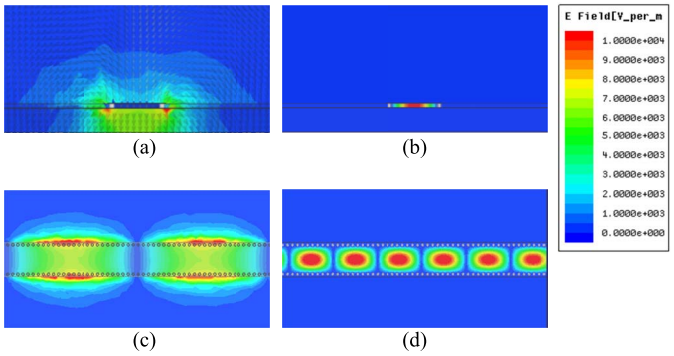

Fig. 2. Simulated electric field distributions of the two modes propagating along the proposed DMC-MSL. (a) Cross section of the quasi-TEM mode. (b) Cross section of the TE_{10}-like mode. (c) Top view of the quasi-TEM mode. (d) Top view of the TE_{10}-like mode.

simulated results are obtained with the help of a commercial full-wave electromagnetic solver Ansys HFSS [31].

B. Operating Principle

Simulated electric field distributions of the two modes transmitting along the DMC-MSL are shown in Fig. 2 to verify the operating principle of the transmission line. As can be seen in Fig. 2(a) and (c), the wave is mainly concentrated in the lower Substrate 2 when the DMC-MSL operates at the low-frequency mode. The electric field distribution is identical to the traditional MSL, which means that it is the quasi-TEM mode. On the other hand, the wave propagates in the SIW integrated in Substrate 1 for the high-frequency mode as shown in Fig. 2(b) and (d). Therefore, the DMC-MSL works in the TE_{10}-like mode.

The characteristics of the DMC-MSL operating in the low-frequency band should be mainly controlled by width W of the metallic strip, thickness h_2 of Substrate 2, and the relative dielectric constant of Substrate 2, which is the same with the conventional MSL [32]. Moreover, because the thickness of Substrate 1 is much smaller in comparison with the operting wavelength in the low-frequency band in this paper, it would not affect the properteis of the quasi-TEM mode remarkablely as will be shown in Section II-C.

On the other hand, as the DMC-MSL works as an SIW at the high-frequency mode, the properties of Substrate 2 would not influence the characteristics of the DMC-MSL operating in the high-frequency band. The frequency range of the SIW only supporting the fundamental TE_{10}-like mode can be determined by choosing width W of the metallic strip and the dielectric constant of Substrate 1. It is noted that diameter D and

TABLE I
DIMENSIONS OF THE DMC-MSL (UNIT: mm)

Parameters	W	p	D	h_1	h_2
Values	3.7	0.55	0.3	0.254	1.524

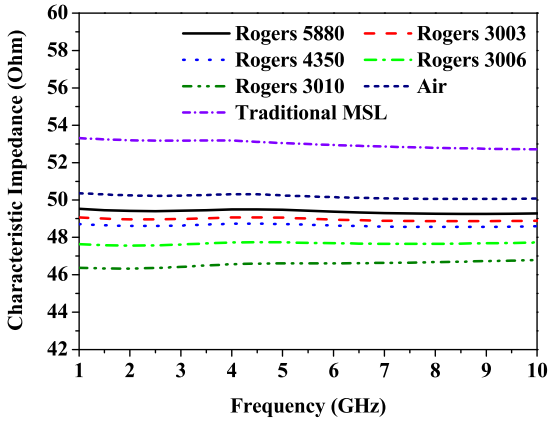

Fig. 3. Simulated characteristic impedance of the DMC-MSL operating in the low-frequency band.

period p of the vias are selected according the design guideline of the SIW previously studied in [33]. The vias are close to the edges of the metallic strip with a spacing of 0.1 mm for ease of fabrication.

C. Dual-Band Performance

Discussions described in Section II-B reveal that W is the parameter that can influence the operating bands of both the low- and high-frequency modes of the DMC-MSL, while other parameters can affect the band of only one mode. In this paper, in order to investigate the performance in the two bands separately, W, h_2, and the permittivity of Substrate 2 are used for determining the band of the quasi-TEM mode of the DMC-MSL first. The band of the TE_{10}-like mode is then tuned by varying the permittivity of Substrate 1. A Rogers 4350 printed circuit board (PCB) laminate with a thickness of 1.524 mm and a dielectric constant of 3.66 is used as Substrate 1. The dimensions of the DMC-MSL are selected to obtain a characteristic impedance of close to 50 Ω for the low-frequency band. Detailed values are listed in Table I. Five types of widely used PCB laminates with different relative dielectric constants and the air are considered here as Substrate 1. The thickness of Substrate 1 is fixed to 0.254 mm. A straight DMC-MSL is performed by utilizing the full-wave simulator.

Fig. 3 presents the simulated characteristic impedances of the DMC-MSL operating in the low-frequency band. The simulated results of the traditional MSL, namely the case of $h_1 = 0$ mm, are also given for comparison. For different dielectric constants of Substrate 1, a minor variation in the characteristic impedance from 46 to 50 Ω can be observed. Moreover, the result of the MSL is 53 Ω, which is slightly larger than those of the DMC-MSL. The small difference can be explained as follows. The existence of Substrate 1 increases the effective width of the metallic strip, which leads to the decrease in the characteristic impedance. The simulated

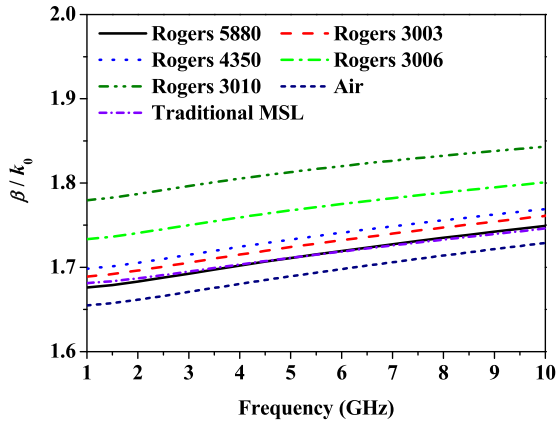

Fig. 4. Simulated normalized propagation constant of the DMC-MSL operating in the low-frequency band.

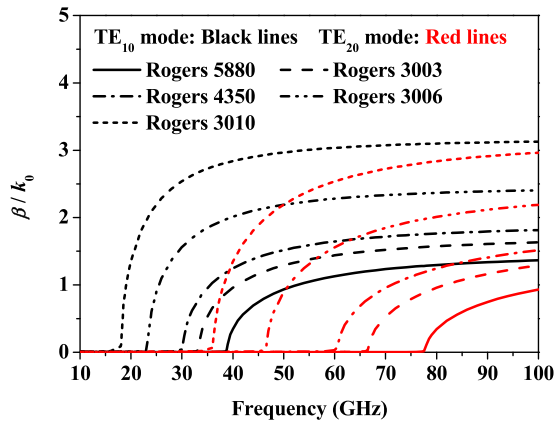

Fig. 5. Simulated normalized propagation constant of the DMC-MSL operating in the high-frequency band.

normalized propagation constants of the DMC-MSL and the MSL are shown in Fig. 4, where a slight increase in the propagation constant with the permittivity of Substrate 1 can be seen. This is because the increase of the permittivity of Substrate 1 can slightly enhance the effective permittivity of the supporting material of the DMC-MSL.

As discussed in Section II-B, the DMC-MSL operates as an SIW in the high-frequency band. Therefore, its transmitting characteristics are the same with those of the conventional SIW that have been investigated in the literature [32]. Here, only the dispersion properties are given in Fig. 5 for the purpose of revealing the operating band of the high-frequency mode of the DMC-MSL. It is observed that with a variation of Substrate 1, the operating band only supporting the fundamental TE_{10}-like mode can be tuned effectively. For Rogers 5880 laminate with the lowest permittivity of 2.2, the high-frequency band of the DMC-MSL is from 39 to 78 GHz, whereas the band for Rogers 3010 with a highest permittivity of 10.2 is from 18 to 36 GHz.

According to the results illustrated in Figs. 3–5, it can be concluded that the characteristics of the DMC-MSL working in the low-frequency band is almost the same as the counterparts of the conventional MSL with identical dimensions. Therefore, the design method of the MSL is still effective

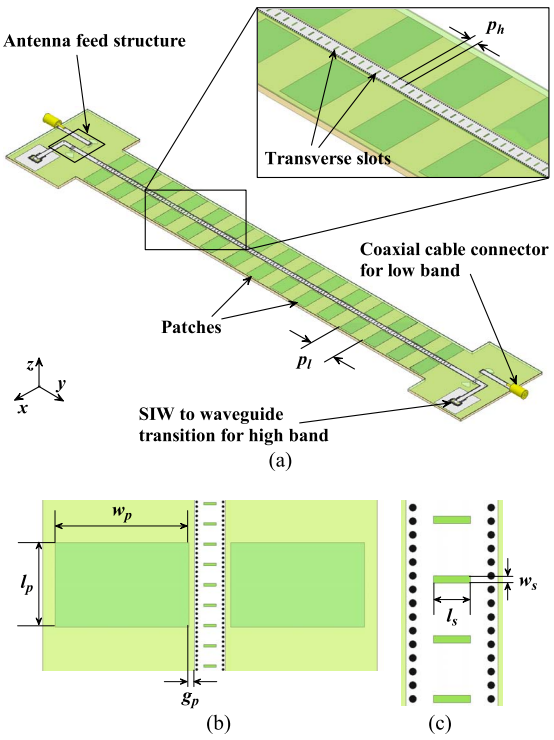

Fig. 6. Geometry of the proposed dual-band leaky-wave antenna. (a) Perspective view. (b) Top view of the microstrip patch unit with dimensions. (c) Top view of the slot unit etched on the SIW with dimensions.

to the DMC-MSL. Furthermore, the variation of the permittivity of Substrate 1 does not affect the properties of the DMC-MSL in the low-frequency band significantly. As a result, the operating band of the high-frequency mode of the DMC-MSL can be adjusted almost independently by changing the permittivity of Substrate 1. Hence, the frequency ratio of the two bands can be tuned flexibly in practical applications.

III. Antenna Design

Based on the DMC-MSL discussed in Section II, a dual-band leaky-wave antenna with a large frequency ratio is designed in this section for microwave and millimeter-wave applications simultaneously. A Rogers 5880 PCB laminate with a thickness of 0.254 mm is selected as Substrate 1 of the antenna, whereas Substrate 2 and the dimensions of the DMC-MSL are the same as those given in Section II.

A. Antenna Geometry

Configuration of the entire antenna is presented in Fig. 6. For the low-frequency band, considering that the propagation constant of the DMC-MSL shown in Fig. 4 is larger than the wave number k_0 in free space, the fundamental quasi-TEM mode propagating along the DMC-MSL cannot generate radiation directly. Therefore, two parasitic microstrip patch arrays with a period of p_l are added on the bottom layer of Substrate 1 to excite the spatial harmonic located in fast-wave region [12]. The length and width of the patches are l_p and w_p, respectively, as depicted in Fig. 6(b). Furthermore, gap g_p between the patches and the DMC-MSL can control the power coupling to the patches. For radiation in the high-frequency band, a slot array with a period of p_h is etched on the DMC-MSL. By properly choosing p_h, radiation from the fundamental TE_{10}-like mode can be achieved according to the theory presented in [17]. The sizes of the slot are l_s and w_s as illustrated in Fig. 6(c). The final values of the configuration parameters of the proposed design are listed in Table II.

TABLE II
Dimensions of the Dual-Band Leaky-Wave Antenna (Unit: mm)

Parameters	p_l	p_h	l_p	w_p	g_p	l_s	w_s
Values	20	2.4	10	16	0.65	1.5	0.3

In order to excite the dual-band leaky-wave antenna in practice, a feeding structure is designed and connected to the two ends of the DMC-MSL. With the help of the antenna feed, the low- and high-frequency bands can be excited separately. Its details will be studied in Section IV.

B. Microstrip Patch Array for Low-Frequency Band

According to Floquet's theorem, a series of space harmonics can be excited by introducing periodic structures to perturb the uniform transmission line. The propagation constant β_m of the mth spatial harmonic in the longitudinal direction, i.e., the y-axis in Fig. 6, can be written by [34]

$$\beta_m = \beta_0 \pm 2m\pi / p \tag{1}$$

where β_0 is the phase constant of the basic mode of the perturbed transmission line, and p is the period of the perturbing structure. Then, the propagation constant η_m of the mth spatial harmonic in the transverse plane, i.e., the xoz plane in Fig. 6, can be given by

$$\eta_m^2 = k_0^2 - \beta_m^2. \tag{2}$$

Therefore, when $\eta_m^2 \le 0$, i.e., $|\beta_m| \ge k_0$, there is no radiation from the mth spatial harmonic.

The leaky-wave antenna without the feed structure parts is simulated first by employing the HFSS simulator. Wave ports connecting to the two ends of the antenna are used as the feed and the load. The propagation constant β_0 of basic mode transmitting along the perturbed DMC-MSL and the attenuation constant α can be determined from the equation [35]

$$S_{21} = e^{-(\alpha + j\beta_0)L}\sqrt{1 - |S_{11}|^2} \tag{3}$$

where L is the total length of the leaky-wave antenna.

The dispersion diagram of the proposed leaky-wave operating in the low-frequency band is depicted in Fig. 7, where the simulated β_0 of the basic mode is larger than k_0. The dispersion curves of the spatial harmonics excited by the periodic patches can be calculated from (1). By setting p_l to 20 mm, it is seen that the -1st spatial harmonic begins to enter the leaky region when $f_{l1} = 5.5$ GHz. Moreover, the radiation from the -2nd harmonic occurs when f_{l3} reaches 10.9 GHz. When $f_{l2} = 8.5$ GHz, β_{-1} equals to 0, which means that the radiation beam directs to the broadside direction. However, due to the open stopband phenomenon of the

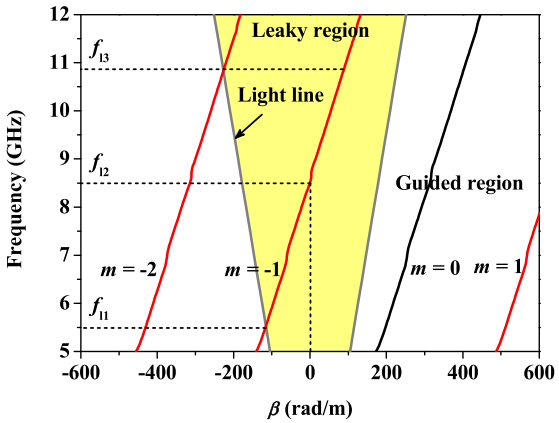

Fig. 7. Dispersion diagram of the proposed dual-band leaky-wave antenna operating in the low-frequency band.

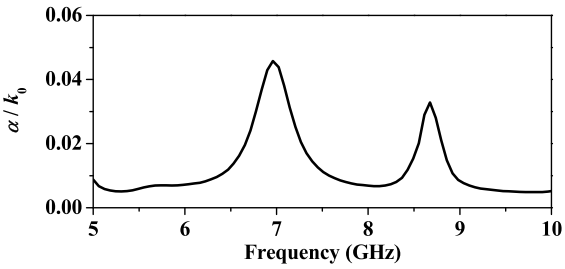

Fig. 8. Simulated normalized attenuation constant of the proposed dual-band leaky-wave antenna operating in the low-frequency band.

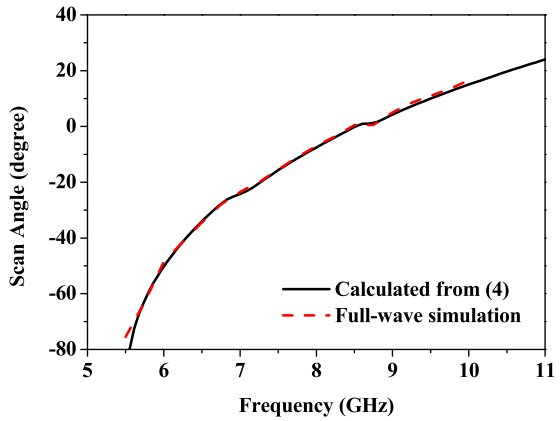

Fig. 9. Calculated and simulated scan angle curves of the proposed leaky-wave antenna operating in the low-frequency band.

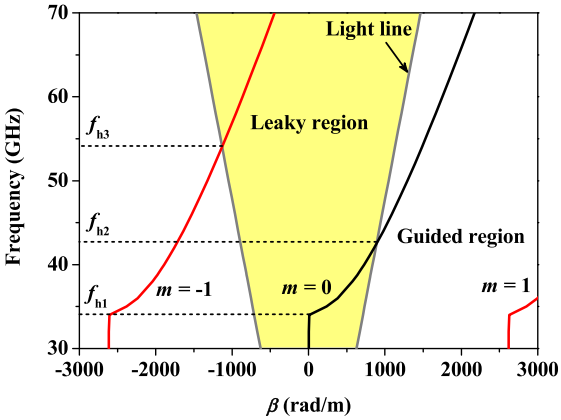

Fig. 10. Dispersion diagram of the proposed dual-band leaky-wave antenna operating in the high-frequency band.

leaky-wave antenna, the reflection coefficient of the antenna should increase at this frequency. It should be noted that due to the excitation of the TM_{10} mode of the metallic patches, a slight disturbance at around 7 GHz can be observed on the dispersion diagram. Furthermore, the simulated normalized attenuation constant of the leaky-wave antenna operating in the low-frequency band is presented in Fig. 8. The attenuation constant is relatively large at the frequencies close to 7 and 8.5 GHz, which is also attributed to the influence of the excitation of the patch mode and the open stopband phenomenon.

Based on the relationship between the propagation constants in the longitudinal direction and the transverse plane, the direction of the radiation beam from the mth harmonic can be given by

$$\theta_m = \sin^{-1}(\beta_m / k_0) \tag{4}$$

where θ_m is the angle measured from the broadside to the beam.

By substituting the simulated results given in Fig. 7 into (4), the curve of θ_m can be calculated theoretically as shown in Fig. 9. The simulated θ_m obtained from the full-wave simulation of the entire antenna structure including the feed parts is also provided in Fig. 9, which agrees well with the calculated one. The radiation beam of the -1st harmonic starts from the backward end-fire direction and then scans to the broadside with the increase of frequency. Similar to the curves in Figs. 7 and 8, the flat response can also be seen at about 7 and 8.5 GHz due to the patch mode and the open stopband.

C. SIW Slot Array for High-Frequency Band

Fig. 10 presents the dispersion diagram of the leaky-wave antenna operating in the high-frequency band. As previously investigated in [17], β_0 of the SIW slot array is increased due to filling with the dielectric material. As shown in Fig. 10, within the frequency range from the cutoff frequency f_{h1} of the leaky waveguide to f_{h2}, β_0 is less than k_0. When the operating frequency further increases, β_0 enters the guided region. Furthermore, radiation from the -1st spatial harmonic emerges when the frequency achieves f_{h3}. For the purpose of getting the single radiation beam over the frequency range from f_{h1} to f_{h2}, p_h with a small value of 2.4 mm is selected. The radiation from the -1st spatial harmonic cannot be excited within the required operating band of the SIW slot array. As shown in Fig. 11, the simulated normalized attenuation constant varies from 0.05 to 0.15 throughout the high-frequency band of the leaky-wave antenna.

Fig. 12 compares the calculated and full-wave simulated curves of θ_m. When frequency varies from 34.8 to 42.6 GHz, the beam of the basic mode can scan from the direction close to the broadside to the forward end-fire direction.

IV. Antenna Feed Design

Feed structure plays a crucial role in the dual-band leaky-wave antenna design. Since the frequency ratio of the two bands is greater than 5, the conventional feeding schemes,

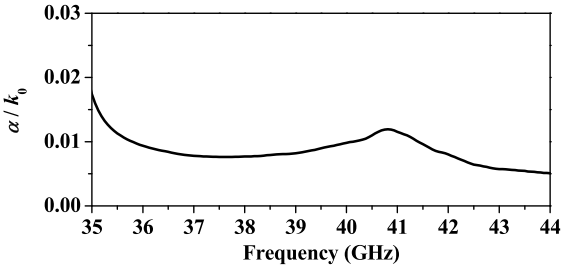

Fig. 11. Simulated normalized attenuation constant of the proposed dual-band leaky-wave antenna operating in the high-frequency band.

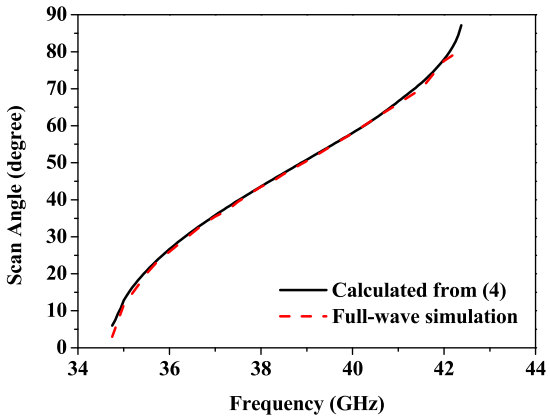

Fig. 12. Calculated and simulated scan angle curves of the proposed leaky-wave antenna operating in the high-frequency band.

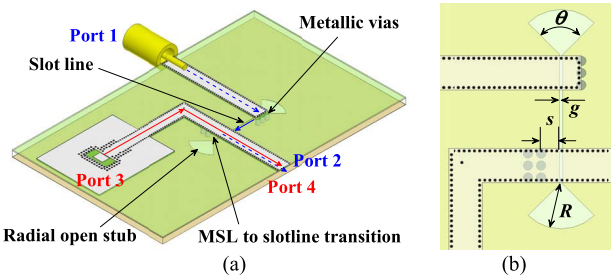

Fig. 13. Geometry of the antenna feed structure. (a) Perspective view. (b) Top view with dimensions.

TABLE III
DIMENSIONS OF THE FEED STRUCTURE

Parameters	R	θ	s	g
Values	5 mm	90°	2.1 mm	0.1 mm

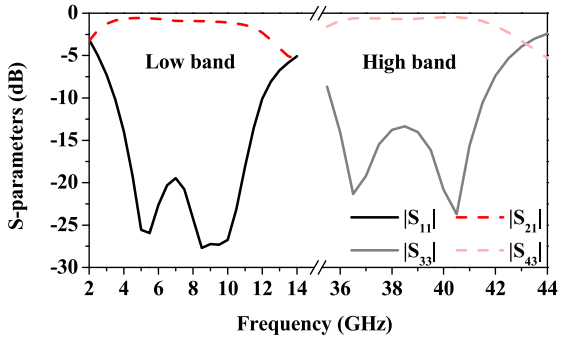

Fig. 14. Simulated S-parameters of the antenna feed structure.

including the coaxial cable connector and the waveguide, are not easy to excite the two bands simultaneously. In order to solve the issue, a novel antenna feed structure having two input ports that can excite the two bands of the antenna separately is proposed in this section. Its geometry is presented in Fig. 13, where Ports 1 and 2 are the input and output ports for the low-frequency band, whereas Ports 3 and 4 are those for the high-frequency band. Two transmission paths for low- and high-frequency waves are described in blue and red arrows in Fig. 13. First, six metallic vias linking the metallic strip of the DMC-MSL with the ground plane of Substrate 2 work as a short circuit for the low-frequency band of the DMC-MSL. Therefore, the extended portion of the DMC-MSL behind the short circuit would not affect the performance of the feeding structure in the low-frequency band. A 90° bend with a wideband SIW to waveguide transition reported in [36] is connected to the metallic strip of the DMC-MSL, which is utilized to feed the leaky-wave antenna operating in the high-frequency band. Second, two back-to-back transitions between the MSL and the slotline are used to couple the low-frequency waves between two shorted-end sections of the DMC-MSL. As a result, the input power from the coaxial cable connector can be transmitted to the DMC-MSL successfully when it operates in the low-frequency band.

In this design, since the cutoff frequency of the TE_{10}-like mode of the DMC-MSL is much higher than the low-frequency band of the antenna, the power from Port 1 cannot transmit in the thin SIW composing the DMC-MSL and be coupled to Ports 3 and 4. On the other hand, the thin SIW can be seen as a closed waveguide structure throughout the operating band if it is designed obeying the rules provided in [33]. Hence, the power fed to Port 3 in the high-frequency band cannot be coupled to Ports 1 and 2 as well.

The final values of the dimensions of the feed structure can be found in Table III. The simulated S-parameters of the proposed antenna feed operating in the two bands are illustrated in Fig. 14. The −10 dB impedance bandwidths of the low- and high-frequency bands are 110% (from 3.5 to 12 GHz) and 15.6% (from 35.6 to 41.6 GHz), respectively. Moreover, the insertion loss of the antenna feed is less than 2.2 and 0.95 dB, respectively, for the low- and high-frequency bands.

V. MEASUREMENT AND DISCUSSION

The proposed dual-band leaky-wave antenna based on the DMC-MSL has been fabricated and measured to demonstrate the design. The top and back views of Substrates 1 and 2 are shown in Fig. 15(a). The SIW working as the metallic strip of the DMC-MSL and the SIW to WR-28 waveguide transitions were designed in Substrate 1. The microstrip patch array has also been etched on the bottom surface of Substrate 1. Moreover, the MSL to slotline transitions were implemented on the bottom surface of Substrate 2. The two substrates glued together were mounted on an aluminium fixture for convenience of measurement. Metallic screws located in the middle

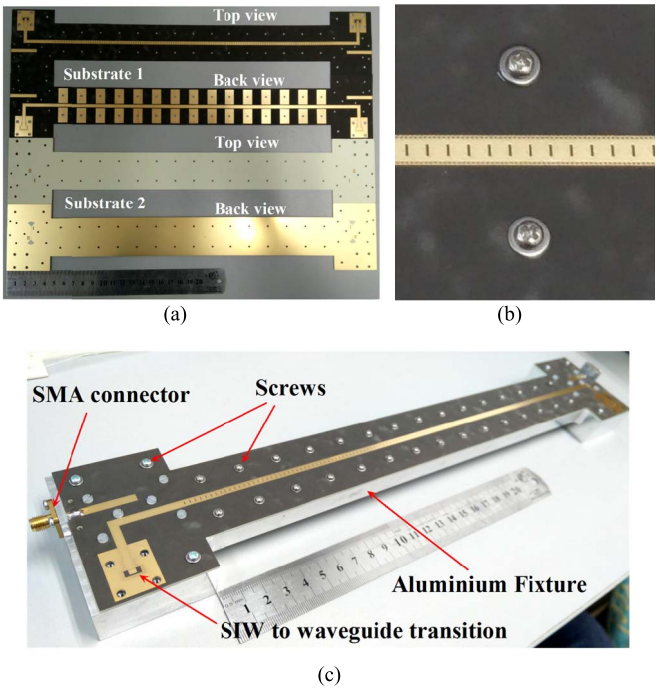

Fig. 15. Photographs of the fabricated dual-band leaky-wave antenna. (a) Top and bottom views of the two substrates. (b) Enlarged view of the SIW slot array. (c) Perspective view of the antenna.

of each microstrip patch were used for alignment but did not affect the characteristics of the patches. The entire geometry of the fabricated prototype is presented in Fig. 15(c). Two SMA connectors were applied to feed the antenna working in the low-frequency band. The S-parameters of the antenna were measured by an Agilent Network Analyzer E8363C, whereas the radiation performance was tested in a far-field anechoic chamber. During radiation performance measurement, a coaxial cable load and a WR-28 waveguide load are connected to Port 2 of the antenna, respectively. The gain of the antenna was achieved by comparing with standard gain horns.

A. S-Parameter

Measured and simulated S-parameters of the leaky-wave antenna operating in the low- and high-frequency bands are illustrated in Fig. 16, where satisfactory agreement between measured and simulated results can be observed. For the low-frequency band, the measured $|S_{11}|$ is below -10 dB throughout the operating band from 5.6 to 8.6 GHz, whereas the simulated -10 dB operating band is from 5.3 to 8.4 GHz. The excitation of the TM_{10} mode from the metallic patches leads to a stronger coupling between the patch array and the DMC-MSL, and thus, lower $|S_{21}|$ can be observed at around 7 GHz. Furthermore, for the high-frequency band, the measured and simulated $|S_{11}|$ is below -10 dB over the operating bands from 35 to 40 GHz and from 36 to 41.4 GHz, respectively. The slight shift in frequency between the measured and simulated results is mainly caused by the fabrication tolerance. On the other hand, the measured $|S_{21}|$ is lower than -6 and -25 dB separately within the low- and high-frequency bands.

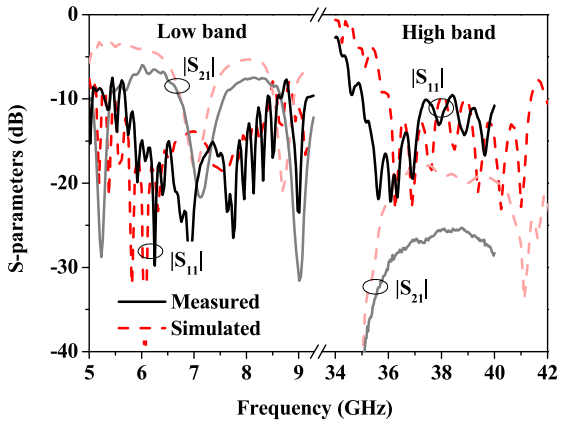

Fig. 16. Measured and simulated S-parameters of the dual-band leaky-wave antenna.

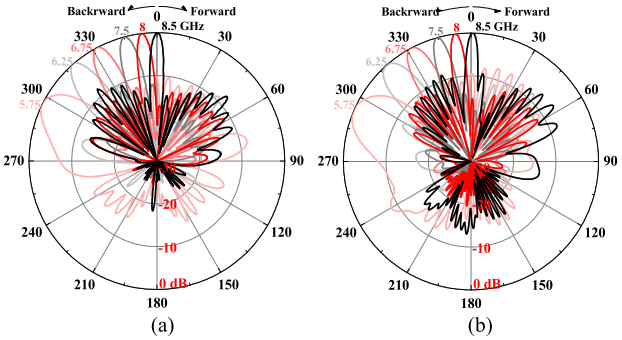

Fig. 17. Measured and simulated low-frequency band radiation patterns in the *yoz* plane. (a) Measured. (b) Simulated.

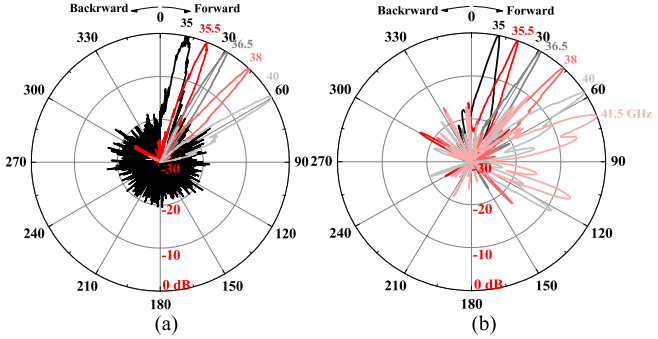

Fig. 18. Measured and simulated high-frequency band radiation patterns in the *yoz* plane. (a) Measured. (b) Simulated.

B. Radiation Pattern

The measured and simulated *yoz* plane radiation patterns of the leaky-wave antenna operating in the low-frequency band are presented in Fig. 17, which are in good agreement. The radiation pattern generated by the -1st spatial harmonic of the microstrip patch array scans from $-64°$ in the backward direction to the broadside direction when the frequency changes from 5.75 to 8.5 GHz. The measured sidelobe level of the radiation pattern is less than -8 dB.

As illustrated in Fig. 18, the measured *yoz* plane radiation pattern of the antenna operating in the high-frequency band is consistent with the simulated one. By employing the basic mode of the SIW slot array, the radiation pattern in the

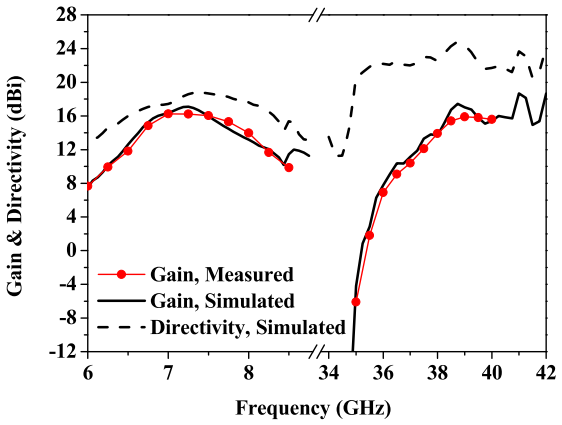

Fig. 19. Measured and simulated gains and simulated directivity of the dual-band leaky-wave antenna.

TABLE IV
COMPARISON BETWEEN PROPOSED AND REPORTED DUAL-BAND LEAKY-WAVE ANTENNAS

Ref.	Transmission line type	Operating frequencies (GHz)		Center freq. ratio	Scanning angle ranges	
		Low band	High band		Low band	High band
[25]	CRLH	5.2-5.7	10.3-11.5	2	-15°~ 45°	-45°~ 15°
[26]	CRLH	8.6-9.5	15-19	1.7	-25°~ 35°	-25°~ 15°
[27]	MNG	3.7-5.5	6.7-10	1.8	-43°~ 73°	-80°~ 83°
[28]	Half-width MSL	5.2-6.4	7.9-9	1.5	30°~ 65°	-46°~ -10°
This work	DMC-MSL	5.8-8.5	35-41.5	5.3	-64°~ 0°	11°~ 70°

high-frequency band directs to forward direction. The radiation beam scans from 11° to 70° for the frequency varying from 35 to 41.5 GHz. Due to the frequency limitation of the used network analyzer, the measured results above 40 GHz are not available. Besides it is noted that the simulated cross-polarization levels of the antenna are less than −19 and −30 dB over the low- and high-frequency bands, respectively.

C. Gain and Directivity

Fig. 19 presents the measured and simulated gains and the simulated directivity for the observed beam maximum of the proposed dual-band leaky-wave antenna. The measured gain is in good agreement compared with the simulated results. The directivity varies from 13 to 18.8 dBi within the operating band from 6 to 8.5 GHz, while the gain is larger than 8 dBi for the low-frequency band. On the other hand, the simulated directivity is higher than 20.5 dBi throughout the high-frequency band. Due to approaching the cutoff frequency of the TE_{10}-like mode propagating along the DMC-MSL, the gain decreases significantly when the frequency is lower than 36 GHz. In addition, a considerable loss of the leaky-wave antenna can be observed in the high-frequency band by comparing the gain with the directivity, which is mainly because the dielectric loss of the SIW operating at millimeter-wave frequencies.

D. Comparison and Discussion

The structure features and performance of the reported dual-band leaky-wave antennas are summarized in Table IV for comparison with this paper. By utilizing the CRLH and MNG transmission lines with more than one leaky-wave range, dual-band leaky-wave antennas are realized in [25]–[27]. The radiation beam scans from backward to forward regions in both of the operating bands. The half-width MSL leaky-wave antenna loaded with periodic U-shaped slots designed in [28] and the design based on the DMC-MSL proposed in this paper also have two bands, but different from the above-mentioned three works, the radiation beam only directs to either forward or backward direction in the two bands. On the other hand, the center frequency ratios of the two bands are around or less than 2 for all the previous antennas. In this paper, with the help of the novel DMC-MSL, a much larger frequency ratio of 5.3 is obtained successfully.

VI. CONCLUSION

The DMC-MSL with a dual-layered geometry that can support the quasi-TEM and TE_{10}-like modes in two operating bands separately has been proposed and investigated. Apart from maintaining the characteristics of the conventional MSL and the SIW, a flexible frequency ratio of the two operating bands has been realized by adjusting the permittivity of the upper dielectric laminate composing the DMC-MSL. A dual-band leaky-wave antenna with a large frequency ratio of 5.3 has been designed, fabricated, and measured based on the DMC-MSL structure. Backward and forward frequency-scanning radiation beams have been demonstrated across the low- and high-frequency bands from 5.75 to 8.5 GHz and from 35 to 41.5 GHz, respectively. The proposed transmission line and antenna structure with the simple planar configuration and a good performance would be attractive for future microwave and millimeter-wave dual-band wireless applications.

REFERENCES

[1] Z. D. Liu, P. S. Hall, and D. Wake, "Dual-frequency planar inverted-F antenna," *IEEE Trans. Antennas Propag.*, vol. 45, no. 10, pp. 1451–1458, Oct. 1997.
[2] Y.-X. Guo, K.-M. Luk, K.-F. Lee, and R. Chair, "A quarter-wave U-shaped patch antenna with two unequal arms for wideband and dual-frequency operation," *IEEE Trans. Antennas Propag.*, vol. 50, no. 8, pp. 1082–1087, Aug. 2002.
[3] B. Li and K. W. Leung, "Strip-fed rectangular dielectric resonator antennas with/without a parasitic patch," *IEEE Trans. Antennas Propag.*, vol. 53, no. 7, pp. 2200–2207, Jul. 2005.
[4] K.-L. Lau and K.-M. Luk, "A wide-band circularly polarized L-probe coupled patch antenna for dual-band operation," *IEEE Trans. Antennas Propag.*, vol. 53, no. 8, pp. 2636–2644, Aug. 2005.
[5] W. Menzel, M. Al-Tikriti, and M. B. E. Lopez, "Common aperture, dual frequency printed antenna (900 MHz and 60 GHz)," *Electron. Lett.*, vol. 37, no. 17, pp. 1059–1060, Aug. 2001.
[6] L. Zhang, K. Y. See, B. Zhang, and Y. P. Zhang, "Integration of dual-band monopole and microstrip grid array for single-chip tri-band application," *IEEE Trans. Antennas Propag.*, vol. 61, no. 1, pp. 439–443, Jan. 2013.

[7] T. Zhihong, Y. P. Zhang, C. Luxey, A. Bisognin, D. Titz, and F. Ferrero, "A ceramic antenna for tri-band radio devices," *IEEE Trans. Antennas Propag.*, vol. 61, no. 11, pp. 5776–5780, Nov. 2013.
[8] L. Y. Feng and K. W. Leung, "Dual-frequency folded-parallel-plate antenna with large frequency ratio," *IEEE Trans. Antennas Propag.*, vol. 64, no. 1, pp. 340–345, Jan. 2016.
[9] D. Wang and C. H. Chan, "Multiband antenna for WiFi and WiGig communications," *IEEE Antennas Wireless Propag. Lett.*, vol. 15, pp. 309–312, 2016.
[10] L. Y. Feng and K. W. Lueng, "Dual-fed hollow dielectric antenna for dual-frequency operation with large frequency ratio," *IEEE Trans. Antennas Propag.*, vol. 65, no. 6, pp. 3308–3313, Jun. 2017.
[11] A. A. Oliner, "Radiating periodic structures: Analysis in terms of k vs. β diagrams," Short Course Microw. Field Netw. Techn., Polytechnic Inst. Brooklyn Graduate Center, New York, NY, USA, Tech. Rep., Jun. 1963.
[12] A. A. Oliner and D. R. Jackson, "Leaky-wave antennas," in *Antenna Engineering Handbook*, J. Volakis, Ed., 4th ed. New York, NY, USA: McGraw-Hill, 2007, ch. 10.
[13] J. H. Wang and K. K. Mei, "Theory and analysis of leaky coaxial cables with periodic slots," *IEEE Trans. Antennas Propag.*, vol. 49, no. 12, pp. 1723–1732, Dec. 2001.
[14] Z. L. Ma and L. J. Jiang, "One-dimensional triple periodic dual-beam microstrip leaky-wave antenna," *IEEE Antennas Wireless Propag. Lett.*, vol. 14, pp. 390–393, 2015.
[15] Z. L. Ma, L. J. Jiang, S. Gupta, and W. E. I. Sha, "Dispersion characteristics analysis of one dimensional multiple periodic structures and their applications to antennas," *IEEE Trans. Antennas Propag.*, vol. 63, no. 1, pp. 113–121, Jan. 2015.
[16] Y. J. Cheng, W. Hong, K. Wu, and Y. Fan, "Millimeter-wave substrate integrated waveguide long slot leaky-wave antennas and two-dimensional multibeam applications," *IEEE Trans. Antennas Propag.*, vol. 59, no. 1, pp. 40–47, Jan. 2011.
[17] J. Liu, D. R. Jackson, and Y. Long, "Substrate integrated waveguide (SIW) leaky-wave antenna with transverse slots," *IEEE Trans. Antennas Propag.*, vol. 60, no. 1, pp. 20–29, Jan. 2012.
[18] J. Liu, D. R. Jackson, Y. Li, C. Zhang, and Y. Long, "Investigations of SIW leaky-wave antenna for endfire-radiation with narrow beam and sidelobe suppression," *IEEE Trans. Antennas Propag.*, vol. 62, no. 9, pp. 4489–4497, Sep. 2014.
[19] S.-T. Yang and H. Ling, "Design of a microstrip leaky-wave antenna for two-dimensional bearing tracking," *IEEE Antennas Wireless Propag. Lett.*, vol. 10, pp. 784–787, 2011.
[20] T.-L. Chen, Y.-D. Lin, and J.-W. Sheen, "Microstrip-fed microstrip second higher order leaky-mode antenna," *IEEE Trans. Antennas Propag.*, vol. 49, no. 6, pp. 855–857, Jun. 2001.
[21] S. Gupta, S. Abielmona, and C. Caloz, "Microwave analog real-time spectrum analyzer (RTSA) based on the spectral-spatial decomposition property of leaky-wave structures," *IEEE Trans. Microw. Theory Techn.*, vol. 57, no. 12, pp. 2989–2999, Dec. 2009.
[22] Y. J. Li and J. H. Wang, "Polarization property of leaky coaxial cable with overlapped triangle slots," *IEEE Antennas Wireless Propag. Lett.*, vol. 9, pp. 1049–1052, 2010.
[23] F. M. Monavar, S. Shamsinejad, R. Mirzavand, J. Melzer, and P. Mousavi, "Beam-steering SIW leaky-wave subarray with flat-topped footprint for 5G applications," *IEEE Trans. Antennas Propag.*, vol. 65, no. 3, pp. 1108–1120, Mar. 2017.
[24] Z. L. Ma, K. B. Ng, C. H. Chan, and L. J. Jiang, "A novel supercell-based dielectric grating dual-beam leaky-wave antenna for 60-GHz applications," *IEEE Trans. Antennas Propag.*, vol. 64, no. 12, pp. 5521–5526, Dec. 2016.
[25] T. Kodera and C. Caloz, "Dual-band full-space scanning leaky-wave antenna based on ferrite-loaded open waveguide," *IEEE Antennas Wireless Propag. Lett.*, vol. 8, pp. 1202–1205, 2009.
[26] J. Machac, M. Polivka, and K. Zemlyakov, "A dual band leaky wave antenna on a CRLH substrate integrated waveguide," *IEEE Trans. Antennas Propag.*, vol. 61, no. 7, pp. 3876–3879, Jul. 2013.
[27] R. B. V. B. Simorangkir and Y. Lee, "A planar dual-band periodic leaky-wave antenna based on a mu-negative (MNG) transmission line," *IEEE Trans. Antennas Propag.*, vol. 63, no. 5, pp. 2370–2374, May 2015.
[28] D. K. Karmokar and K. P. Esselle, "Periodic U-slot-loaded dual-band half-width microstrip leaky-wave antennas for forward and backward beam scanning," *IEEE Trans. Antennas Propag.*, vol. 63, no. 12, pp. 5372–5381, Dec. 2015.
[29] F. Fesharaki, T. Djerafi, M. Chaker, and K. Wu, "Low-loss and low-dispersion transmission line over DC-to-THz spectrum," *IEEE Trans. THz Sci. Technol.*, vol. 6, no. 4, pp. 611–618, Jul. 2016.
[30] J. P. Guo, T. Djerafi, and K. Wu, "Mode composite waveguide," *IEEE Trans. Microw. Theory Techn.*, vol. 64, no. 10, pp. 3187–3197, Oct. 2016.
[31] Ansoft Corp., Canonsburg, PA, USA. *HFSS: High Frequency Structure Simulator Based on the Finite Element Method*. [Online]. Available: http://www.ansoft.com/
[32] D. M. Pozar, *Microwave Engineering*, 3rd ed. New York, NY, USA: Wiley, 2004.
[33] D. Deslandes and K. Wu, "Accurate modeling, wave mechanisms, and design considerations of a substrate integrated waveguide," *IEEE Trans. Microw. Theory Techn.*, vol. 54, no. 6, pp. 2516–2526, Jun. 2006.
[34] R. E. Collin, *Foundations for Microwave Engineering*. New York, NY, USA: McGraw-Hill, 1992.
[35] K. Wei, Z. Zhang, Z. Feng, and M. F. Iskander, "Periodic leaky-wave antenna array with horizontally polarized omnidirectional pattern," *IEEE Trans. Antennas Propag.*, vol. 60, no. 7, pp. 3165–3173, Jul. 2012.
[36] Y. Li and K.-M. Luk, "60-GHz dual-polarized two-dimensional switch-beam wideband antenna array of aperture-coupled magneto-electric dipoles," *IEEE Trans. Antennas Propag.*, vol. 64, no. 2, pp. 554–563, Feb. 2016.

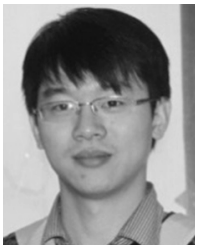

Yujian Li (S'12–M'15) was born in Hunan, China, in 1987. He received the B.S. and M.S. degrees in communications engineering from Beijing Jiaotong University, Beijing, China, in 2009 and 2012, respectively, and the Ph.D. degree in electronic engineering from the City University of Hong Kong, Hong Kong, in 2015.

He joined the Institute of Lightwave Technology, Beijing Jiaotong University, in 2015, as an Associate Professor. His current research interests include millimeter wave antennas, base station antennas, and leaky wave structures.

Dr. Li received the Outstanding Research Thesis Award from the City University of Hong Kong in 2015. He received the Best Paper Award at the 2015 IEEE Asia–Pacific Conference on Antennas and Propagation, the Best Student Paper Award at the 2013 National Conference on Antennas, and the Best Student Paper Award (Second Prize) at the 2013 IEEE International Workshop on Electromagnetics. He was selected as a Finalist in the student paper contest of the 2015 IEEE Antennas and Propagation Society Symposium on Antennas and Propagation. He has served as a Reviewer for the IEEE TRANSACTIONS ON ANTENNAS AND PROPAGATION, the IEEE ANTENNAS AND WIRELESS PROPAGATION LETTERS, and the *IET Microwaves, Antennas and Propagation*.

Junhong Wang (M'02–SM'03) was born in Jiangsu, China, in 1965. He received the B.S. and M.S. degrees in electrical engineering from the University of Electronic Science and Technology of China, Chengdu, China, in 1988 and 1991, respectively, and the Ph.D. degree in electrical engineering from Southwest Jiaotong University, Chengdu, in 1994.

In 1995, he joined as a Faculty Member with the Department of Electrical Engineering, Beijing Jiaotong University, Beijing, China, where he became a Professor in 1999. From 1999 to 2000, he was a Research Associate with the Department of Electric Engineering, City University of Hong Kong, Hong Kong. From 2002 to 2003, he was a Research Scientist with the Temasek Laboratories, National University of Singapore, Singapore. He is currently with the Key Laboratory of all Optical Network and Advanced Telecommunication Network, Ministry of Education of China, Beijing Jiaotong Univeristy, and also with the Institute of Lightwave Technology, Beijing Jiaotong University. His current research interests include numerical methods, antennas, scattering, and leaky wave structures.